Impact of ionic strength and surface charge on ceramic membrane fouling by oil-in-water emulsions

A quantitative analysis using DLVO and XDLVO models

Qin, Guangze; Zhou, Hanxiao; Tanis, Begüm; Rietveld, Luuk C.; Heijman, Sebastiaan G.J.

DOI
10.1016/j.seppur.2025.133424

Publication date
2025

Document Version
Final published version

Published in
Separation and Purification Technology

Separation and Purification Technology 372 (2025) 133424

Contents lists available at ScienceDirect

Separation and Purification Technology

journal homepage: www.elsevier.com/locate/seppur

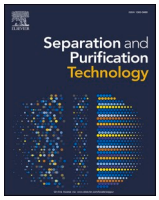

Impact of ionic strength and surface charge on ceramic membrane fouling by oil-in-water emulsions: A quantitative analysis using DLVO and XDLVO models☆

Guangze Qin *, Hanxiao Zhou, Begüm Tanis, Luuk C. Rietveld, Sebastiaan G.J. Heijman

Section of Sanitary Engineering, Department of Water Management, Faculty of Civil Engineering and Geosciences, Delft University of Technology, Stevinweg 1, 2628 CN Delft, the Netherlands

ARTICLE INFO

Editor: Dr. B. Van der Bruggen

Keywords:
Membrane fouling
DLVO model
XDLVO model
Surface charge
Hydrophilicity
Oil-in-water emulsion
Silicon carbide membrane

ABSTRACT

Large amounts of oily wastewater, which can be defined as produced water, are generated in oilfields. Ultrafiltration (UF) serves as an effective and economical method to purify produced water. Unfortunately, membrane fouling during produced water treatment is severe. In this paper, the effects of the ionic strength (1, 20, and 100 mM) as well as different surfactants on the membrane fouling are investigated. Four surfactants, including SDS (anionic), APG (non-ionic), CTAB (cationic) and DDAPS (zwitterionic), were selected for this study. The Derjaguin-Landau-Verwey-Overbeek (DLVO) and extended DLVO (XDLVO) models were used to quantify interactions between the membrane-oil droplet and deposited oil layer-oil droplet surfaces and to compare these interactions with the fouling experiments. The (X)DLVO interaction energies of the membrane-oil droplet exhibited a strong agreement with the fouling tendencies at 1 mM salinity. The SiC-deposited (B20) membrane showed less reversible and irreversible membrane fouling than the Al_2O_3 (B0) membrane when filtering negatively charged O/W emulsions stabilized with SDS, APG, or DDAPS. The DLVO model predicted a higher fouling tendency at higher salinity levels during the filtration of SDS, APG, or DDAPS-stabilized O/W emulsions and a decreased fouling tendency for CTAB-stabilized emulsion with the B20 membrane. However, at higher salinity levels, the XDLVO energy barrier was affected by both the repulsive electrostatic double layer (EL) interaction and attractive Lewis acid-base (AB) interaction. By comparing both experiments and (X)DLVO modeling, this study improves the fundamental understanding of the effect of ionic strength and surfactant types on reversible and irreversible fouling of the Al_2O_3 and SiC-coated membranes fouling by O/W emulsions.

1. Introduction

Large quantities of produced water are discharged concurrently with oil and gas extraction at a global average rate of about 39.75 million m^3 per day [1,2]. Several studies have investigated various treatment techniques to enhance produced water reuse including Microfiltration (MF) [3], ultrafiltration (UF) [4], electroflocculation [5], reverse electrodialysis (ED) [6], membrane distillation [7,8], adsorption [9], sand filtration [10], gas flotation [11], chemical precipitation [12], and advanced oxidation [13]. However, among other water treatment technologies, UF is considered to be the most promising approach for removing oil, grease, and colloidal particle removal, making it an effective pretreatment option for the reuse of the produced water [4,14].

The main challenge with the use of UF membranes for produced water treatment is fouling, which occurs due to the aggregation of oil droplets on the surface or in the membrane pores. To effectively control membrane fouling, it is crucial to understand the oil droplet-membrane interactions and oil droplet-oil layer interactions. Here, the presence of surfactants, used during oil extraction, is considered to play a vital role [15]. Surfactants absorb on both the oil–water interface of the droplets and the membrane surface. Therefore, the surfactants influence both the interactions between the oil droplets and membrane surface and the oil droplet-oil layer interactions. Sodium dodecyl sulfate (SDS, anionic), alkyl polyglycoside (APG, non-ionic), and cetyltrimethylammonium bromide (CTAB, cationic) are frequently used in oil extraction [16–18], allowing for a more practical investigation of the membrane fouling

☆ This article is part of a special issue entitled: 'EuroMembrane 2024 (invited only)' published in Separation and Purification Technology.

* Corresponding author.
E-mail address: G.Qin@tudelft.nl (G. Qin).

https://doi.org/10.1016/j.seppur.2025.133424
Received 1 February 2025; Received in revised form 9 April 2025; Accepted 5 May 2025
Available online 10 May 2025

mechanism. However, previous research by De Vos et al. has highlighted the advantage of the application of zwitterionic surfactants, such as N-dodecyl-N,N-dimethyl-3-ammonio-1-propanesulfonate (DDAPS), due to its low fouling propensity under high salt concentrations [19–21]. The Derjaguin-Landau-Verwey-Overbeek (DLVO) theory has been widely used in various fouling studies. However, it sometimes falls short of accurately describing interactions at shorter separation distances between two surfaces. To address this limitation, the Lewis acid-base (AB) interaction, which accounts for electron donor–acceptor interactions at distances less than 10 nm, was integrated into the DLVO model, resulting in the extended DLVO (XDLVO) model [22]. While the XDLVO model is more commonly employed than the DLVO model to analyze colloidal fouling on membrane surfaces, its application to apolar foulants, such as oil, remains less thoroughly understood. Previous studies have typically focused on either the effects of different surfactants at a single salinity level or on oil–water emulsions with varying salinity without considering surfactants variations [17,23]. He et al., e.g., reported that for oil-in-water (O/W) emulsions stabilized by the non-ionic surfactant (Triton ^{TM} X-100), the interaction energies predicted by the DLVO model were consistent with the fouling tendencies at various salinities for the polyvinylidene fluoride (PVDF) MF membrane in the constant flux filtration mode [23]. The group of Chew reported that the DLVO correlated well with the fouling tendencies, rather than the XDLVO model, for the filtration of the O/W emulsion stabilized with SDS, CTAB and Tween 20 for the 0.22 μm PVDF membrane in the constant pressure filtration mode [17]. However, Zhang et al. reported that the fouling tendency for a Span 80-stabilized O/W emulsion mismatched with the DLVO/XDLVO model for the polyethersulfone (PES) UF membrane in the constant pressure filtration mode [24].

Silicon carbide (SiC) and alumina (Al_2O_3) ceramic membranes are commercially available and widely used in wastewater treatment applications, standing out among other ceramic membranes [25–29]. Increasing the adsorption-free energy between oil and the membrane alleviates membrane fouling by changing the membranes' hydrophilicity and surface zeta potentials. Therefore, SiC membranes are preferred over Al_2O_3 for produced water treatment due to their super hydrophilic and highly negatively charged surface [30]. To the best of our knowledge, no prior studies have quantitatively analyzed and compared fouling by O/W emulsions with the DLVO and XDLVO models using these specific membrane materials. This study is the first to examine the combined impact of both varying salinities and different surfactants, utilizing positively charged Al_2O_3 membranes and negatively charged SiC ceramic membranes by combining fouling experiments and the DLVO/XDLVO model. Various studies focused on the relationship between the DLVO/XDLVO model and membrane fouling in the dead-end constant pressure mode [17,24,31]. However, there are limited studies on fouling in the crossflow constant flux mode for the separation of O/W emulsion [32,33], although this is the operational mode in full-scale installations. The filtration experiments were conducted in the constant flux crossflow mode, assessing how membrane surface properties and emulsion characteristics, such as salinity levels and surfactant types, affect membrane fouling. Additionally, the study explored the relationship between the DLVO/XDLVO models and the reversible and irreversible fouling.

Reversible fouling, namely cake layer fouling, has been the subject of several studies [34–36]. A practical and cost-effective method is to differentiate between reversible and irreversible fouling is to backwash the membrane with demineralized (DI) water. The extent of reversible and irreversible fouling can then be calculated based on the resistance-in-series model [37,38]. To the authors' knowledge, this is the first time that a study was performed, combining constant flux, backwashing (related to the reversible and irreversible fouling) and DLVO theory. This integration provides a comprehensive understanding of fouling behavior under practical operating conditions in full scale application.

Consequently, the objective of the present is to enhance the fundamental understanding of the interaction between oil droplets and ceramic membranes in the crossflow constant flux mode, with a focus on studying the correlation between the DLVO/ XDLVO interaction energy and reversible and irreversible fouling, varying salinity and surfactant types.

2. Materials and methods

2.1. Materials

N-hexadecane (296317), sodium dodecyl sulfate (SDS, L4509-250G), APG (49122), Hexadecyltrimethylammonium bromide (CTAB, H5882), DDAPS (≥97 %, 40232) and sodium chloride (S9998-1KG), which were supplied by Sigma-Aldrich Co., Ltd, the Netherlands, were used for the preparation of the O/W emulsions.

SiC-deposited Al_2O_3 membranes were obtained via low-pressure chemical vapor deposition (LPCVD), as reported in our previous studies [30]. The tubular Al_2O_3 membranes, provided by the CoorsTek Co., Ltd, were chosen as substrate for LPCVD with permeabilities in the 350 ± 10 Lm^{-2} h^{-1} bar^{-1} range. Polycrystalline 3C-SiC was coated on Al_2O_3 membranes using two precursors (SiH_2Cl_2 and C_2H_2) with coating time of 20 min at a temperature of 860 °C via LPCVD. The membranes without coating and those with a coating time of 20 min were labeled as B0 and B20, respectively. The pore size of the B0 and B20 membrane were 41 nm and 33 nm, respectively, as determined from our previously reported results [30].

2.2. Membrane characterization

Surface SEM images of the B0 and B20 membrane was obtained by NovaNanoLab 600 (FEI company, USA). The water contact angle (WCA) of both the pristine B0 membranes and the LPCVD-coated B20 membranes was performed by a contact angle instrument (Dataphysics OCA25, Germany). The WCA measurements were performed by the sessile drop method by dosing 2 μl liquid (ultrapure water, formamide, diiodomethane) on the flat sheet membrane surface. Each measurement was repeated five times per sample, and average values were obtained for the surface tension component calculation. Detailed information on the WCA measurements can be found in Text S1. The zeta potential of both B0 and B20 membranes was measured with an electrokinetic analyzer (SurPASS 3, Anton-Paar, Graz, Austria). However, the membrane zeta potential could not be measured in electrolyte solutions with high concentrations (e.g., 100 mM NaCl) because of the range limit (<50 mM NaCl) of the SurPASS electrokinetic analyzer. Hence, the Freundlich ion adsorption model was used to estimate ζ_m at 100 mM NaCl concentration [23,39].

2.3. Oil-in-water emulsions

To study the effect of the charge of the emulsions on membrane fouling, various micro-sized O/W emulsions were prepared for the membrane fouling experiments. These included an anionic SDS-stabilized emulsion, a non-ionic APG-stabilized emulsion, a zwitterionic DDAPS-stabilized emulsion, and a cationic CTAB-stabilized emulsion. To prepare a 500 mg/L SDS stabilized emulsion, 2 g N-hexadecane and, 956.4 mg SDS were added into 1L of deionized (DI) water. The mixture was stirred continuously at 1500 rpm using a magnetic stirrer (C-MAG HS 10, IKA, the Netherlands) for twelve hours, followed by ultrasonication using a Branson Ultrasonics sonifier (CPX3800H, USA) for two hours, as described in previous studies [40–42]. A fresh emulsion was prepared by diluting 1 L of O/W emulsion with 3 L of DI water, ensuring a consistent oil concentration of 500 mg/L. This concentration aligns with the typical oil and grease content of 100–1000 mg/L in oily wastewater [43]. To prepare 4 L of O/W emulsions with salinity concentrations of 1 mM, 20 mM, and 100 mM, 0.234 g, 4.68 g, and 23.38 g of NaCl were added, respectively. The same preparation method was used for the preparation of the APG, DDAPS, and CTAB-

based emulsions. O/W emulsions were prepared using 0.1 times the critical micelle concentration (CMC) of each surfactant. The CMC values for SDS, APG, CTAB, and DDAPS were 2391 mg/L, 348 mg/L, 346 mg/L, and 1006 mg/L [19,44], respectively. For a total emulsion volume of 4 L, the corresponding amounts of used surfactants were 957.6 mg for SDS, 139.2 mg for APG, 138.4 mg for CTAB, and 402.4 mg for DDAPS, respectively. The micro-sized oil droplets and their distributions were analyzed using a particle size analyzer (Bluewave, Microtrac, USA), while the emulsions' zeta potential was measured with a Malvern Zetasizer Advance analyzer (Zetasizer Lab, Malvern, UK).

2.4. Filtration experiments with mico-sized O/W emulsions

A constant permeate flux crossflow setup was used for O/W emulsion fouling filtration experiments (Fig.S1). A constant flux of 80 Lm^{-2} h^{-1} (Fig.S2) was maintained by a digital feed pump (DDA12-10, Grundfos, Denmark). This flux was estimated based on the threshold flux determined though the conventional flux stepping method [30,45,46]. The fouling resistance was calculated according to the resistance-in-series model [37,38]. Detailed information about the filtration protocol can be found in the Supporting Information (Text S2).

2.5. DLVO and XDLVO models

According to classical DLVO theory, the total interaction energy between an oil droplet and the B0 or B20 membrane is expressed as the combination of the Lifshitz-van der Waals (LW) interaction energy and the electrostatic double layer (EL) interaction energy [47]:

$$U_{mlo}^{DLVO}(h) = U_{mlo}^{LW}(h) + U_{mlo}^{EL}(h) \tag{1}$$

Where $U_{mlo}^{DLVO}(h)$ is the total interaction energy between the B0/ B20 membrane (m) and an oil droplet (o), immersed in a surfactant solution (l); h is the separation distance between the oil droplet and B0/B20 membrane; $U_{mlo}^{LW}(h)$ is the LW interaction term and, $U_{mlo}^{EL}(h)$ is the EL interaction term. In addition to the LW and EL interaction energies, the AB interaction energy can also be considered in energy balances for aqueous systems because of the hydrogen bonds in polar liquids like water [17]. The XDLVO model includes the AB interaction component and can be written as:

$$U_{mlo}^{XDLVO}(h) = U_{mlo}^{LW}(h) + U_{mlo}^{EL}(h) + U_{mlo}^{AB}(h) \tag{2}$$

Where $U_{mlo}^{XDLVO}(h)$ is the total interaction energy between the B0/B20 membrane and oil droplet immersed in the surfactant solution, and $U_{mlo}^{AB}(h)$ is the AB interaction term.

$\Delta G_{mlo}^{LW}(h_0)$, $\Delta G_{mlo}^{EL}(h_0)$ and $\Delta G_{mlo}^{AB}(h_0)$ denote the adhesion energies per unit area for LW, EL, and AB interactions, respectively, between two infinite planar surfaces [17,47–49]:

$$\Delta G_{mlo}^{LW}(h_0) = -2\left(\sqrt{\gamma_m^{LW}} - \sqrt{\gamma_l^{LW}}\right)\left(\sqrt{\gamma_o^{LW}} - \sqrt{\gamma_l^{LW}}\right) \tag{3}$$

$$\Delta G_{mlo}^{EL}(h_0) = \frac{\varepsilon_0 \varepsilon_r \kappa}{2}\left(\zeta_m^2 + \zeta_o^2\right)\left[1 - \coth(\kappa h_0) + \frac{2\zeta_m\zeta_o}{\left(\zeta_m^2 + \zeta_o^2\right)}\operatorname{csch}(\kappa h_0)\right] \tag{4}$$

$$\Delta G_{mlo}^{AB}(h_0) = 2\left[\sqrt{\gamma_l^+}\left(\sqrt{\gamma_o^-} + \sqrt{\gamma_m^-} - \sqrt{\gamma_l^-}\right) + \sqrt{\gamma_l^-}\left(\sqrt{\gamma_o^+} + \sqrt{\gamma_m^+} - \sqrt{\gamma_l^+}\right) - \sqrt{\gamma_o^-\gamma_m^+} - \sqrt{\gamma_o^+\gamma_m^-}\right] \tag{5}$$

Where h_0 is the minimum equilibrium cut-off distance, which is 0.158 nm [50], ε_0 is the permittivity of the vacuum, which is 8.8542 *10^{-8} F/M, ε_r is the relative permittivity of water, ζ_m and ζ_o are the zeta potentials of the B0/B20 membrane and the oil droplets, respectively. The three unknown surface tension parameters of the membrane surface (γ_m^{LW}, γ_m^-, γ_m^+) can be determined by measuring the contact angle of three probe liquids with known surface tension (γ_l) and surface tension parameters (γ_l^{LW}, γ_l^+, γ_l^-), as shown in Table.S1. Detailed information about the calculation is provided in the supporting information (Text.S3).

To calculate the real interaction energy between the B0/B20 membrane and a spherical oil droplet, the Derjaguin approximation is used to calculate the corresponding interaction energy between a flat membrane and a spherical oil droplet [47]:

$$U_{mlo}^{LW}(h) = 2\pi\Delta G^{LW}(h_0)\frac{{h_0}^2 a}{h} \tag{6}$$

$$U_{mlo}^{EL}(h) = \pi\varepsilon_0\varepsilon_r a[2\zeta_m\zeta_o\ln(\frac{1+e^{-\kappa d}}{1-e^{-\kappa d}}) + (\zeta_m^2 + \zeta_o^2)\ln(1-e^{-2\kappa d})] \tag{7}$$

$$U_{mlo}^{AB}(h) = 2\pi a\lambda\Delta G^{AB}(h_0)\exp\left(\frac{h_0 - h}{\lambda}\right) \tag{8}$$

Where a is the radius of the oil droplet, h is the surface separation distance between the B0/B20 membrane and a spherical oil droplet, and λ is defined as 0.6 nm, representing the characteristic decay length of AB interactions [17]. The DLVO/XDLVO interaction energies and surface tension components were calculated using MATLAB software (Matlab R2020b).

3. Results and discussion

3.1. Emulsion properties

The particle size distribution of the oil droplets stabilized with various salinity levels and surfactant type is shown in Table.S2. With increasing salinity and varying surfactant types, the particle size distribution of the emulsions kept constant, with an average particle size of 5 ± 1 μm. In addition, the absolute value of the zeta potential of the emulsions decreased with the salinity (Fig. 1), due to the compression of the diffuse double layer. The charge screening effect of the compressed diffuse double layer decreases the absolute zeta potential, by diminishing the electric field and thus reducing the electrophoretic mobility of the emulsion droplets [51]. Additionally, the colloidal stability of the emulsion may decrease, as Na^+ ions reduce the electrostatic repulsion between oil droplets [52].

3.2. Hydrophilicity and zeta potential of the membranes

The effects of the types of surfactants and various salinity levels on

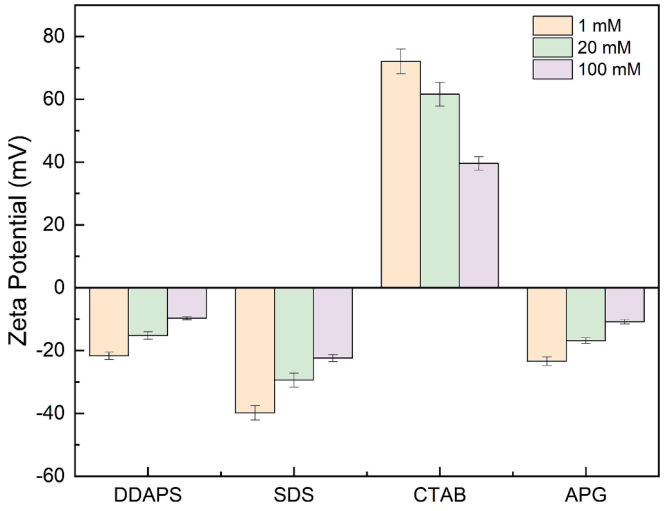

Fig. 1. ζ_o of the O/W emulsions stabilized with various surfactants in various ionic strength (1, 20, and 100 mM).

fouling of the B0 membrane and the B20 membrane were examined using four types of surfactants (SDS, APG, CTAB, and DDAPS) at the salinity levels of 1 mM, 20 mM, and 100 mM. The Freundlich ion adsorption model was used to estimate ζ_m at 100 mM NaCl concentration, which is outside the experimental range of the Surpass equipment (Fig. S3). The absolute value of the zeta potential of the membranes decreased with increasing salinity, regardless of the types of surfactant, for both the B0 and B20 membranes (Fig. 2).

When a layer of SiC was coated, the total surface tension increased, showing stronger intermolecular forces than the pristine Al_2O_3 membrane [53]. Particularly, the enhanced electron donor surface tension component (γ^-) suggests a stronger affinity between water molecules and the material [54] due to the higher presence of the oxygen-containing functional group (–OH) in the B20 membranes. Moreover, the B20 membranes had a higher acid-base component (γ_{AB}), indicating the increased polarity of the membranes. The polarity of a material is generally related to its hydrophilicity. Al_2O_3 is a highly polar compound due to the abundance of hydroxyl groups on its surface, which readily form hydrogen bonds with water molecules, giving it a hydrophilic nature [55]. SiC, on the other hand, is relatively less polar, but its surface tends to oxidize, forming a silicon dioxide layer, which introduces polar functional groups to the surface. These oxide layers increase the hydrophilicity of SiC [56,57], making it more hydrophilic than the Al_2O_3 membrane. This is confirmed by the decrease in the WCA from 36.8°± 0.9° for the B0 membrane to 19.1° ± 0.5° for the B20 membranes, respectively (Fig.S4). Therefore, the increased hydrophilicity and polarity from SiC coating help reduce membrane fouling caused by the oil droplets.

3.3. Comparison of fouling at various salinities

Regarding the 1 mM salinity, Fig. 3 shows that the B20 membrane exhibited less fouling compared to the B0 membrane when filtrating O/W emulsions stabilized with SDS, APG, or DDAPS. However, the B0 membrane showed less fouling than the B20 membrane when filtrating the O/W emulsions stabilized with CTAB. The electrostatic repulsion and attraction between the membrane and oil droplets, the degree of hydrophilicity of the membrane surface, and surfactant adsorption were used to illustrate this phenomenon. The B0 membrane was positively charged at a pH of 5.8 [30,58], and the zeta potential of the B0 membrane shifted from positive to negative when immersed in 0.1 Critical micelle concentration (CMC) solutions of SDS, APG, and DDAPS (Fig. 2), while the highly negatively charged B20 membrane showed no charge inversion when immersed in the 0.1 CMC solutions of positively charged

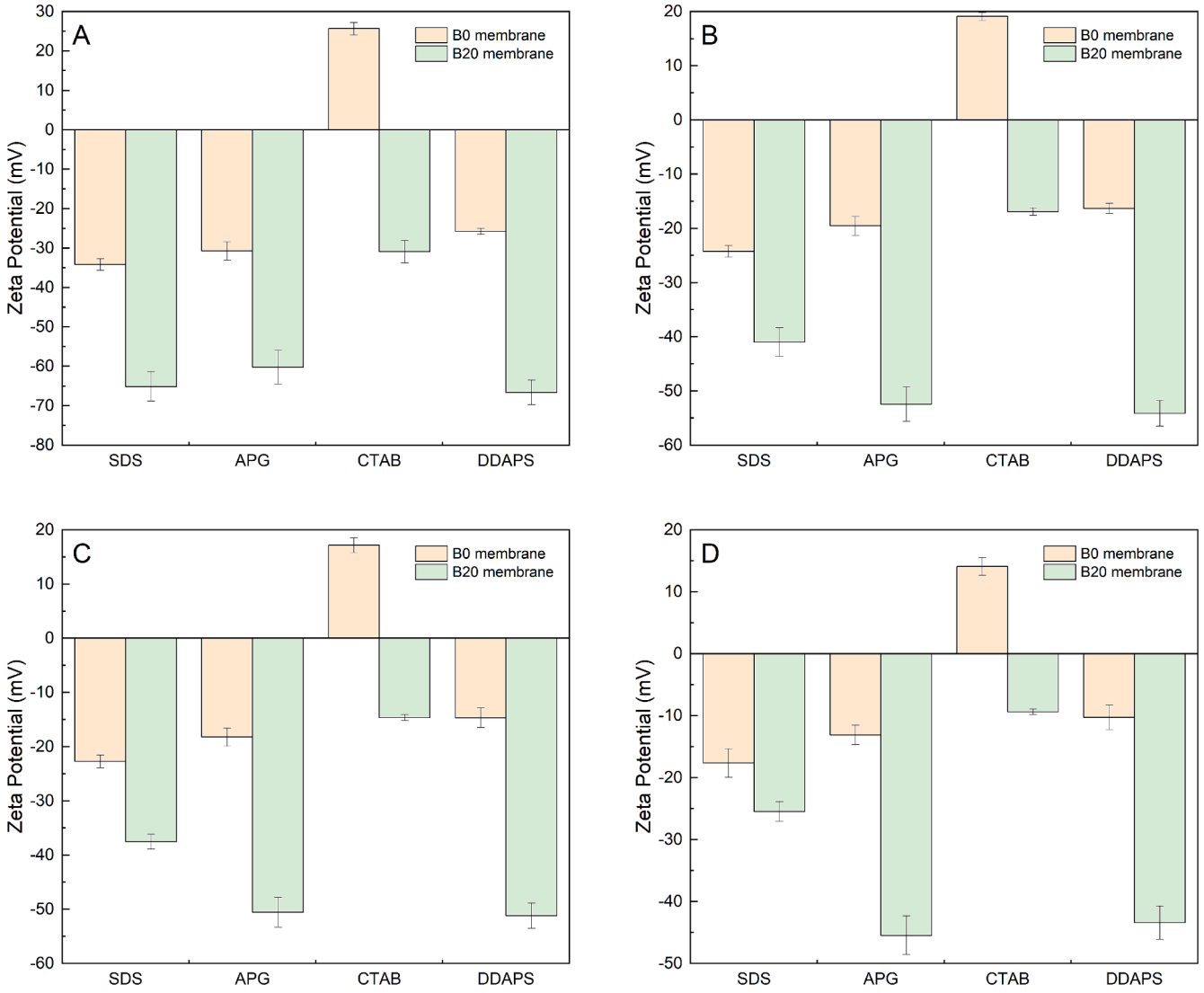

Fig. 2. ζ_i of the B0 membrane and the B20 membrane immersed in different surfactant solutions (SDS, APG, CTAB, or DDAPS) with different salinity: (a)1 mM, (b)10 mM, (c) 20 mM, and (d)100 mM.

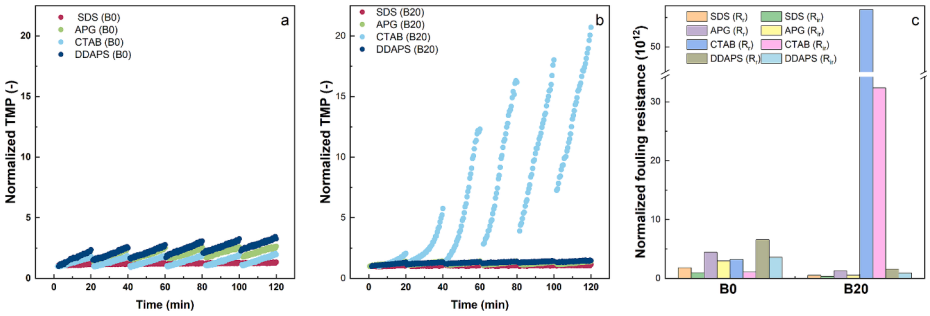

Fig. 3. The normalized fouling curve of (a) B0 membrane and (b) B20 membrane when filtering micro-sized SDS, APG, CTAB, DDAPS stabilized O/W emulsion at the 1 mM salinity; (c) is the normalized fouling resistance of the B0 and B20 membrane at the 1 mM salinity.

CTAB. Additionally, its zeta potential was much more negative than that of the Al_2O_3 membrane using four types of surfactant solutions. When dealing with negatively charged O/W emulsions stabilized with SDS, APG, or DDAPS, the SiC-deposited membrane showed less membrane fouling due to the enhanced electrostatic repulsion between the B20 membrane and O/W emulsions compared to the B0 membrane. However, when filtrating the CTAB-stabilized O/W emulsion which was positively charged, electrostatic repulsion occurred between the positively charged B0 membrane and CTAB-stabilized O/W emulsions. In contrast, the B20 membrane experienced electrostatic attraction with the CTAB-stabilized O/W emulsions, leading to greater fouling than the B0 membrane. From the normalized TMP curve (Fig. 3a-b), the B0 membrane showed a higher fouling tendency compared with the B20 membrane when filtering O/W emulsions stabilized with SDS, APG, or DDAPS, but a lower fouling tendency for CTAB-stabilized O/W emulsions. As shown in Fig. 3c, the B20 membrane showed less total and reversible and irreversible fouling resistance when dealing with the O/W emulsions stabilized with SDS, APG, or DDAPS. When filtrating O/W emulsions stabilized with CTAB, B20 membranes exhibited more fouling than B0 membranes, with the reversible fouling dominant (Fig. 3c), likely due to cake filtration, which can be removed through hydraulic backwash.

When the concentration of NaCl increased from 1 mM to 20 mM (Fig. 4) and then to 100 mM (Fig. 5), both membranes (B0 and B20) showed an increased fouling when filtrating SDS, APG, and DDAPS-stabilized O/W emulsions. At the same time, the surface tension of oil droplets decreased, making oil droplets more prone to deformation and coalescence, which led to increased irreversible fouling [16]. Although, the B20 membrane still exhibited less fouling than the B0 membrane when filtrating SDS, APG, and DDAPS-stabilized O/W emulsions, the B20 membrane, when filtering the CTAB-stabilized O/W emulsion, showed less fouling, compared to the conditions at 1 mM salinity due to the lower electrostatic attraction, but still had more fouling than the B0 membrane. As shown in Fig. 1 and Fig. 2, lower absolute zeta potentials of O/W emulsions and membranes were observed at 20 mM salinity compared to 1 mM salinity due to the charge screening effect [19]. So both the electrostatic repulsion and electrostatic attraction would decrease with the increase in the salinity. Fig. 4a-b and Fig. 5a-b showed that the membrane fouling trend for both B0 and B20 membranes also remained consistent at the higher salinity levels (20 mM, 100 mM) compared to the fouling observed at 1 mM salinity. The fouling order for the B0 membrane was SDS < CTAB < APG < DDAPS, while for the B20 membrane, it was SDS < APG < DDAPS < CTAB (Fig. 4c and Fig. 5c). This can, again, be explained by the electrostatic interactions. Notably, the increased irreversible fouling of the B0 and B20 membrane with increasing salinity can be explained by the decreased charge repulsion. At low salinity, apparently, there was a strong electrostatic repulsion between DDAPS-stabilized droplets and the B20 membrane, as well as a strong electrostatic attraction between CTAB-stabilized droplets and the B20 membrane. However, as salinity increased, both interactions weakened, which means that the strong electrostatic attraction (CTAB) became weaker, and the strong electrostatic repulsion (DDAPS) also diminished. Consequently, the difference in fouling between the two emulsions became less obvious at higher salinity. At the higher salinities, the normalized TMP of the B20 membrane was much lower than that of the B0 membrane when filtrating SDS, APG, and DDAPS-stabilized O/W emulsions, while it was higher than that of the B0 membrane when dealing with CTAB-stabilized O/W emulsions, hence the B20 membrane had better performance when filtrating SDS, APG and DDAPS-stabilized O/W emulsions at 20 mM and 100 mM salinity.

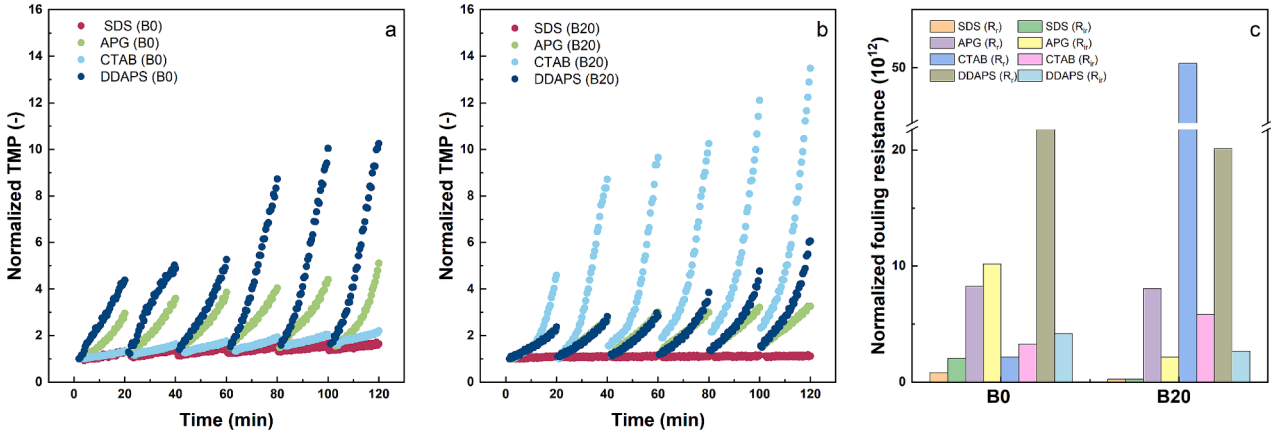

Fig. 4. The normalized fouling curve of (a) B0 membrane and (b) B20 membrane when filtering micro-sized SDS, APG, CTAB, DDAPS stabilized O/W emulsion at the 20 mM salinity; (c) is the normalized fouling resistance of the B0 and B20 membrane at the 20 mM salinity.

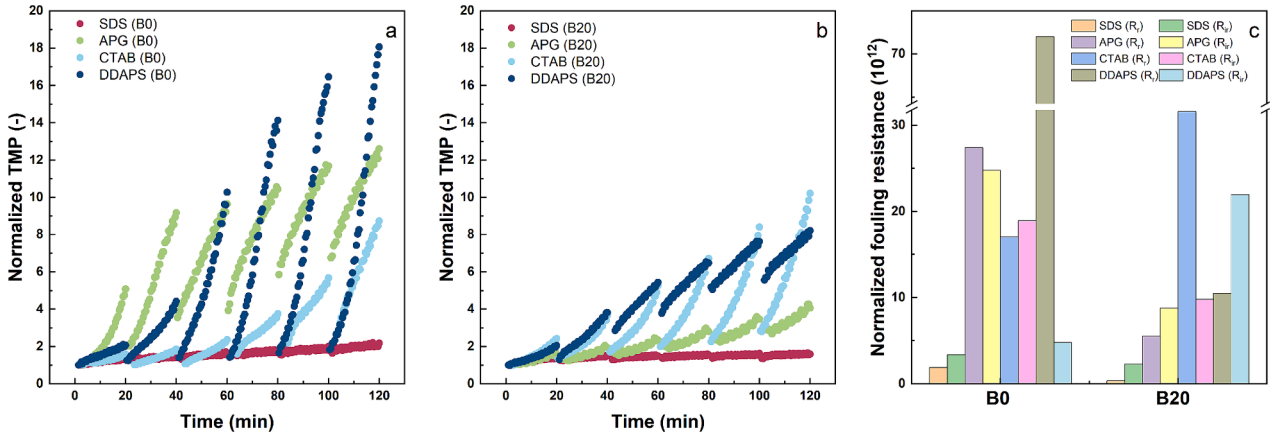

Fig. 5. The normalized fouling curve of (a) B0 membrane and (b) B20 membrane when filtering micro-sized SDS, APG, CTAB, DDAPS stabilized O/W emulsion at the 100 mM salinity; (c) is the normalized fouling resistance of the B0 and B20 membrane at the 100 mM salinity.

3.4. DLVO and XDLVO models

3.4.1. Interaction between membrane and oil droplets

The contact angle and zeta potential of the B0 and B20 membranes, as well as the oil droplets, were measured to calculate the interaction energy between the oil droplets and the surface of the B0 and B20 membranes. The interaction energy components versus the separation distance at the salinity of 1 mM are shown in Fig. 6. The negative value of the interaction energy means an attractive force and the higher the absolute negative value thus indicates severe fouling. Specifically, the LW and AB interactions energies between the B0 and the B20 membranes and oil droplets were attractive at separation distances smaller than 10 nm and 3 nm (Fig. 6a and 6c), respectively, indicating an attractive adhesion force. However, as shown in Fig. 6b, the EL energy for the B20 membrane was repulsive and long-range (<50 nm) due to the negative charge of both the membrane surface and the oil droplets. Therefore, overcoming the electrostatic repulsion requires sufficient energy to bring the oil droplets closer to the membrane surface. The B20 membrane, having a more negative zeta potential, thus displayed a stronger electrostatic double-layer repulsion than the B0 membrane. Additionally, the higher zeta potential enhanced the repulsion of negatively charged oil droplets, potentially improving the antifouling ability of the membranes. The DLVO energy barrier values of the B20 membrane for the SDS, APG, and DDAPS stabilized emulsions were 7529, 5230, and 3282 KT (Fig. 6d), respectively, indicating the lowest fouling potential for SDS-stabilized emulsions, due to the higher energy barrier. The trend of the DLVO energy values is consistent with the fouling tendencies discussed in Section 3.3. For the B0 membrane, the DLVO energy barrier values were 4536, 2876, and 1778 KT for the SDS, APG, and DDAPS surfactants, respectively. The lower energy barrier for the B0 membrane compared to B20 membrane indicates a higher membrane fouling potential. By comparison, for the positively charged CTAB-stabilized emulsions, no energy barrier was observed at the B20 membrane, indicating a high potential. The LW and AB attractive interactions effectively neutralized the EL repulsive interaction, enabling the oil droplets to overcome the energy barrier and facilitating their adhesion onto the surfaces of the B0 and B20 membranes. Therefore, oil droplets stabilized with negatively charged SDS, APG, and DDAPS faced a higher energy barrier before being adsorbed onto the surface of the B0 and B20 membranes.

With the increase in salinity from 1 mM to 100 mM, the DLVO model still maintains a good agreement with the increased membrane fouling, can be confirmed by the decreased energy barrier. The DLVO energy barrier is associate with the energy barrier of the EL component (Fig. 6d,

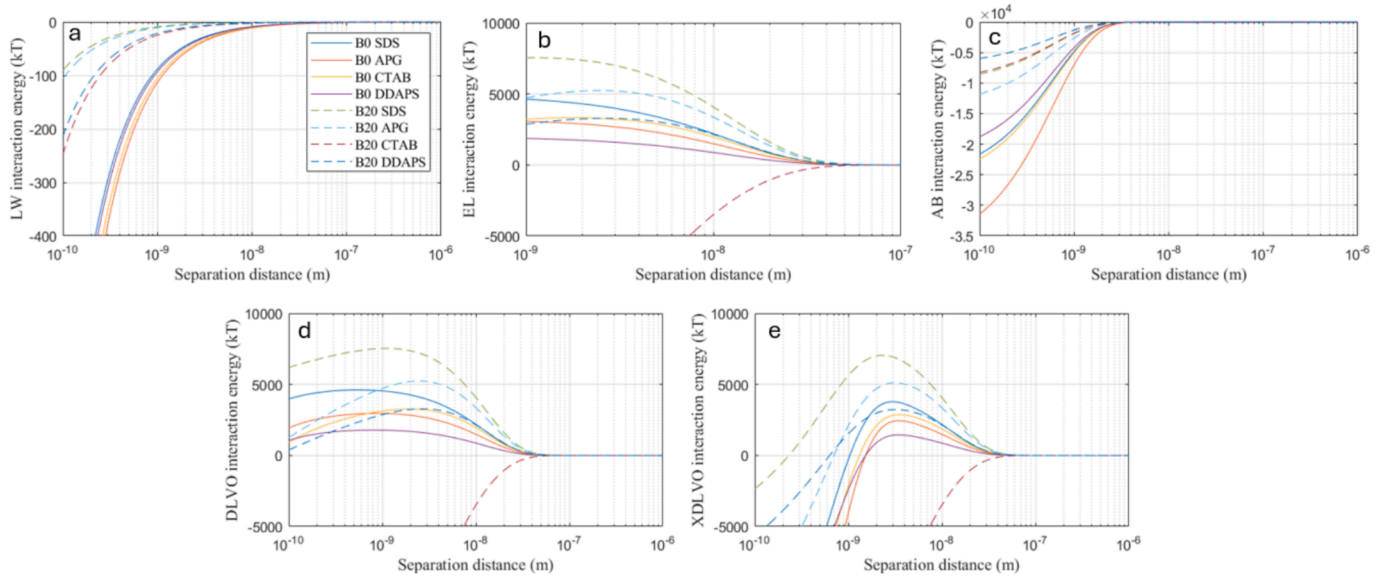

Fig. 6. Effect of surfactants on membrane-oil droplet ineraction energy for B0 and B20 membranes: (a) LW, (b) EL, (c) AB, (d) DLVO, and (e) XDLVO interaction energy at 1 mM salinity.

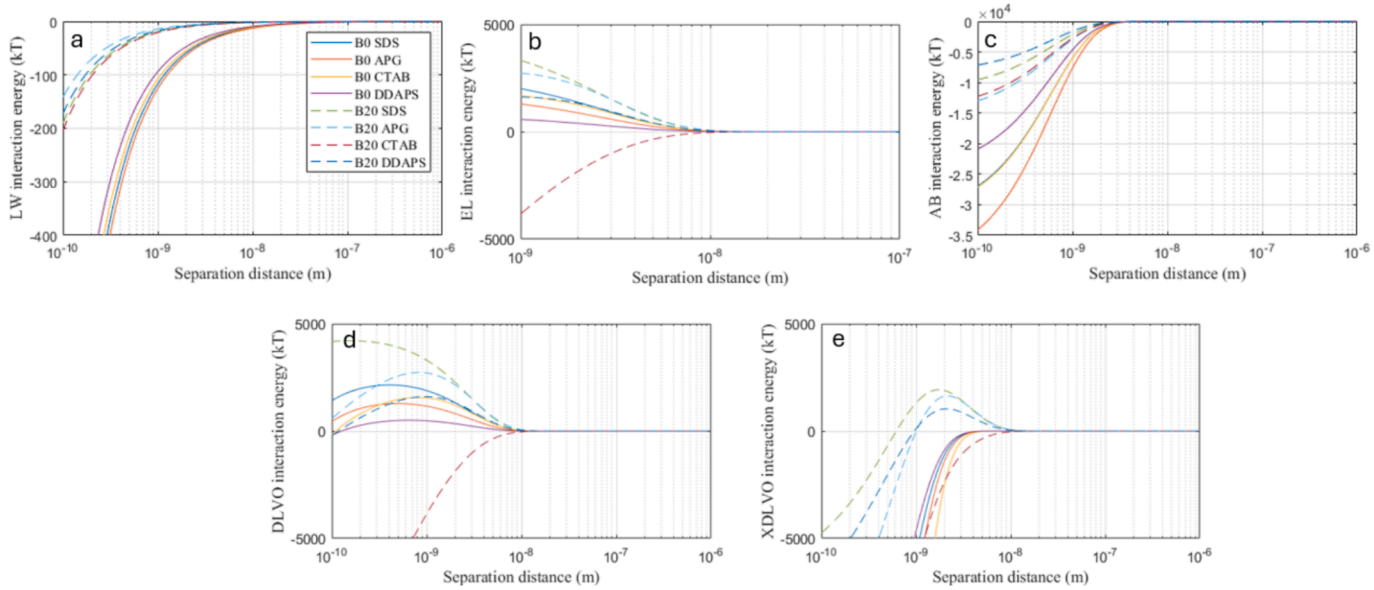

Fig. 7. Effect of surfactants on membrane-oil droplet interaction energy for B0 and B20 membranes: (a) LW, (b) EL, (c) AB, (d) DLVO and (e) XDLVO interaction energy at 20 mM salinity.

Fig. 7d, and Fig. 8d). In other words, the electrostatic interaction energy plays a vital role for the fouling tendencies of the negatively charged B0 membranes and B20 membranes. Zhao et al. also reported that EL interaction is crucial for the anti-fouling ability of the ceramic membranes, especially for the low-pressure gravity-driven system [59]. As shown in Table.S3 and Table.S4, the reduction of the Lewis base (γ^-), from 47.22 to 43.04 for the B0 membrane and 57.42 to 55.22 for the B20 membrane with a salinity increase from 1 mM to 100 mM, respectively, caused lower membrane fouling. Zhao et al. indicated that γ^- is an indicator of membrane fouling. They explain that the larger the value of γ^-, the greater the total interfacial energy, and the smaller the membrane fouling [60]. Therefore, the increase in salinity reduced the electron donor tension on the membrane surface, thus, decreasing the fouling resistance of the B0 and the B20 membrane.

Based on the XDLVO model, the lower negative value of the AB component for the B20 membrane compared to the B0 membranes indicates a lower attractive AB force (Fig. 6c, Fig. 7c, and Fig. 8c). This also contributed to less fouling of the B20 membrane than of the B0 membrane. Current literature on membrane fabrication or modification also suggests that reducing WCA (θ_w) can increase hydrophilicity and the AB interaction energy, thereby mitigating membrane fouling [36,61]. Thus, as salinity increases, the absolute value of the AB component decreased. However, when comparing membrane fouling under different surfactants and salinity levels, the trend of the AB component was not aligned with that of the membrane fouling curve (Fig. 3c, Fig. 4c, Fig. 5c, Fig. 6c, Fig. 7c, and Fig. 8c). One possible explanation is that the differences in WCAs are not significant enough to effectively distinguish the fouling caused by different surfactants. At the salinity of 1 mM, when filtering SDS stabilized emulsions, the B0 and the B20 membrane showed XDLVO energy barriers of 3779 kT and 7046 kT, respectively (Fig. 6e). However, at high salinity levels (20 and 100 mM), the interfacial energy barrier of the B0 membrane disappeared as the

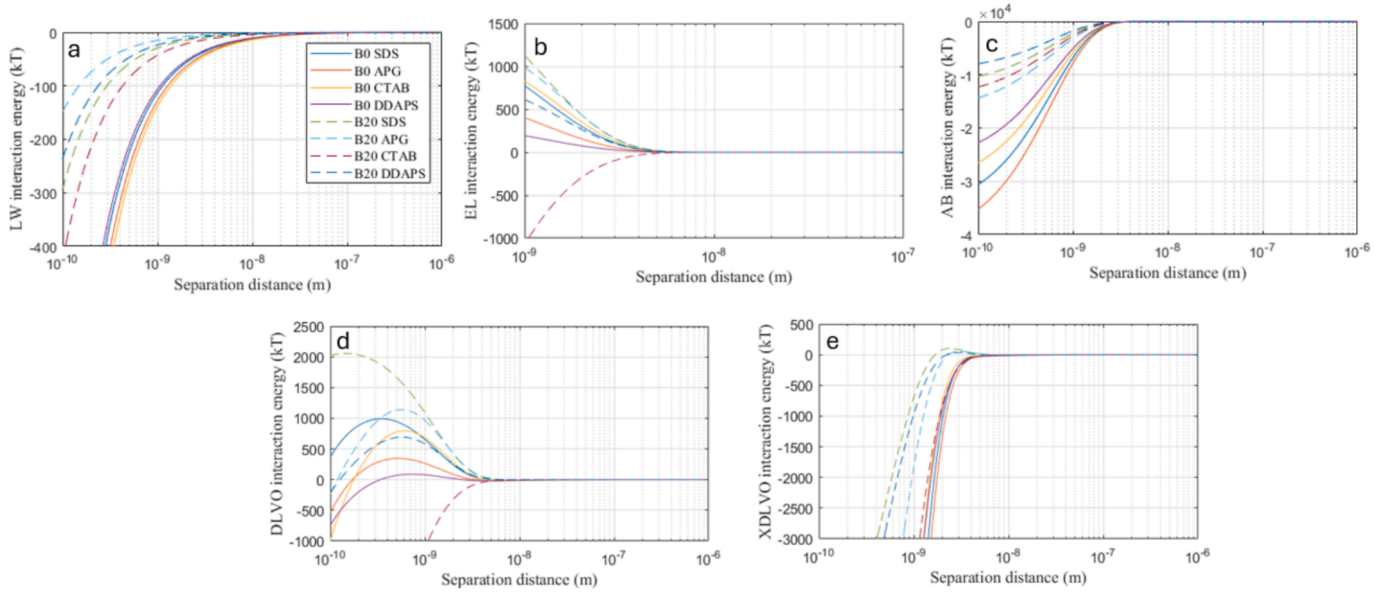

Fig. 8. Effect of surfactants on membrane-oil droplet interaction energy for B0 and B20 membranes: (a) LW, (b) EL, (c) AB, (d) DLVO and (e) XDLVO interaction energy at 100 mM salinity.

XDLVO interaction energy became negative and the energy barrier of the B20 membrane still existed, with values of 1927 kT and 93 kT, respectively (Fig. 7e, and Fig. 8e). The reason is that the interfacial energy barrier of the XDLVO model depends on the EL component at low salinity (1 mM). However, due to the higher charge screening effects caused by high salinity (20 mM, 100 mM), the EL interaction energy was decreased significantly. At the same time, the Debye length, calculated as 9.6 nm at the salinity of 1 mM and 0.956 nm at the salinity of 100 mM [62], respectively, decreased, indicating that at high salinity, the electrostatic interaction played a role at a shorter distance, thus, the energy barrier affected by the both the repulsive EL interaction and attractive AB interactions. Specifically, for the B0 membrane, the dominance the AB interaction was due to the diminished XDLVO energy barrier whereas for the B20 membrane, the EL interaction prevailed since the energy barrier was positive. A similar phenomenon was observed with the other negatively charged emulsions (APG and DDAPS), confirming the anti-fouling ability of the B20 membrane under varying salinity levels and different surfactant types. Thus, the increased B20 membrane fouling can be explained by the reduction in the energy barrier due to increased salinity. When filtering the SDS-stabilized emulsion through the B0 membrane, the energy barrier also diminished and eventually disappeared with the increase in salinity from 1 mM to 100 mM, respectively. For example, as shown in Fig. 6e and Fig. 8e, at a separation distance of 2 nm, which was close to the separation distance corresponding to the energy barrier of the B20 membrane at 1 mM salinity level, the corresponding interaction energy of B0 membrane was 3375 kT at 1 mM and then decreased to −1023 kT (100 mM), indicating that the attractive interactions between the oil droplets and the membrane surface became stronger, thereby, potentially, intensifying membrane fouling. The XDLVO model, thus, accurately predicted the fouling tendency of the B0 and B20 membrane at the salinity of 1 mM, based on the energy barrier values whereas at high salinities (20 mM, 100 mM), due to the dominance of the AB component, a mismatch between the fouling tendency and XDLVO occurred for the B0 membrane. It can be inferred that at low salinity levels, the interaction between oil droplets and the membrane surface was primarily governed by electrostatic forces, while at high salinity levels, adhesion behavior was mainly driven by AB interactions.

To further evaluate the effect of salinity on various interactions, in addition to analyzing the DLVO/XDLVO curves and energy barriers, we also examined the interfacial free energy components of the micro-sized oil droplets and B0/B20 membranes at a separation distance of 0.158 nm. There, the impact of electrostatic free energy (ΔG^{EL}) on the overall interfacial free energy (ΔG^{TOT}) was minimal, given its long-range properties. At low salinity (1 mM), as shown in Table.S5, the B0 membrane exhibited the highest ΔG^{TOT} ($-9.37 mJ/m^2$), e.g. compared to 100 mM salinity (-10.71 mJ/m^2), consistent with the increased membrane fouling observed at high salinity (Fig. 5). The Lifshitz–van der Waals Free Energy (ΔG^{LW}) values remained nearly unchanged across different salinities (ranging from -0.93 to -1.03 mJ/m^2) (Table.S5), indicating that salinity has a limited effect on van der Waals interactions. This aligns with the findings of Xie et al., who reported that van der Waals interactions are insensitive to the variation in electrolyte type, concentration, and pH [63]. At low salinity, after SiC deposition, the absolute value of the LW component ($-0.093 mJ/m^2$) was lower for the B20 membrane than for the B0 membrane (Table.S6). This is because the weaker dispersion forces between the surface of B20 membrane and the liquid reduced the tendency of the liquid to maintain a spherical shape on the surface, making it easier for the liquid to spread, resulting in a more hydrophilic surface. Meanwhile, the Acid-Base Free Energy (ΔG^{AB}) increased considerably from -8.44 mJ/m^2 (B0) to -2.71 mJ/m^2 (B20), indicating that fouling caused by acid-base interactions was effectively reduced after SiC deposition. A similar phenomenon was observed at high salinities (Table S5 and S6). The increase in ΔG^{AB} at different salinities suggests that SiC deposition enhanced the interaction between surface functional (hydroxide) groups and polar water molecules [64]. This enhancement is primarily due to hydrogen bonding interactions between water molecules and electron-donating (γ^+) or accepting (γ^-) groups. These stronger interactions create a high surface energy, which effectively resists fouling [65].

3.4.2. Interaction between deposited oil layer and oil droplet

With the increase in filtration time, the oil droplets aggregated, eventually forming a cake layer to serve as an extra filter layer. The oil droplet-oil droplet interaction was determined entirely by the properties of the oil rather than the membrane characteristics. Thus, when the cake layer was formed, the same zeta potentials and contact angles resulted in an overlap of the DLVO and XDLVO curves for the fouled B0 and B20 membranes (Fig. 9 and Fig.S5). As shown in Fig. 9, when the cake layer was formed, the influence range of each energy component varied. All three interaction energies decreased to zero as the separation distance increased, but the ranges of their influence varied. For both fouled

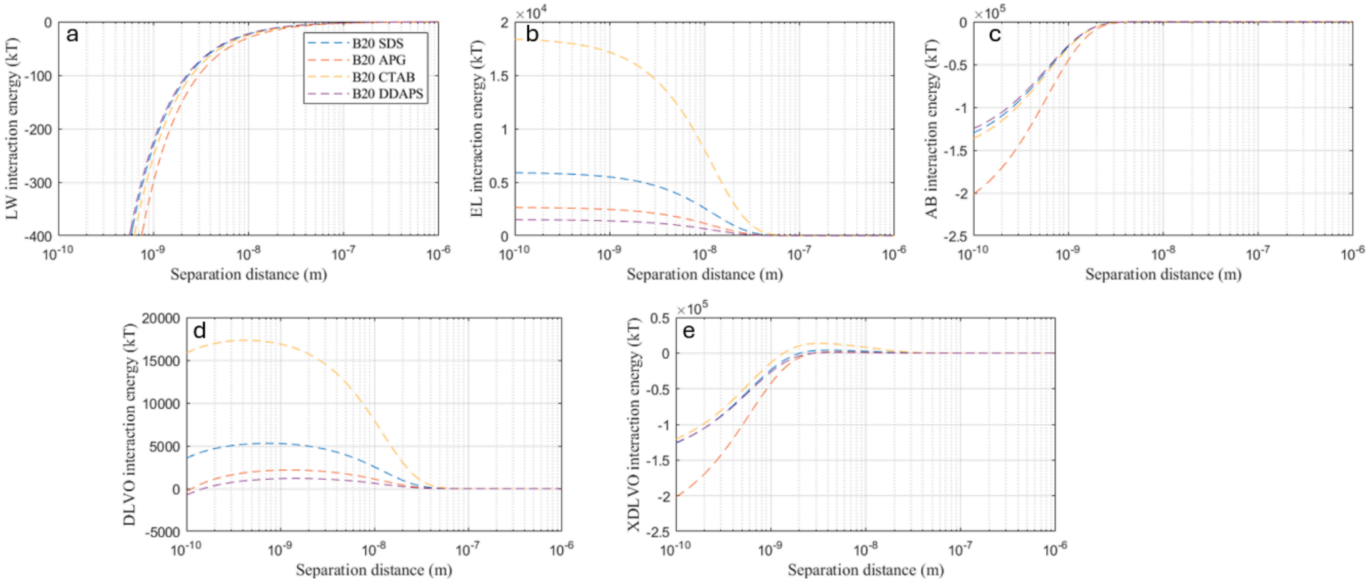

Fig. 9. Effect of surfactants on the deposited oil layer-oil droplet interaction energy for the B20 membrane: (a) LW, (b) EL, (c) AB, and (d) DLVO, and (e) XDLVO interaction energy at 1 mM salinity.

membranes, the influence range of the EL component was the then longest (Fig. 9b), with magnitudes decreasing to 0 at d ≥ 60 nm, while the AB (Fig. 9c) surpassed the EL and LW interactions and dominated the curve of attraction and repulsion at a separation distance smaller than 3 nm. This can be explained by the hydrophobicity of the oil cake layer and the corresponding improved AB interfacial force [66]. Fig. 9d shows that oil droplets stabilized with CTAB had to overcome the largest energy barrier to adsorb or deposit on the oil layer, followed by SDS, APG, and DDAPS. The reason is that the absolute value of the CTAB stabilized oil droplets was the largest, contributing to the larger EL component, which was dominant in the DLVO interaction. The energy barrier of the oil-membrane interaction was thus lower than that for the oil droplet-oil layer interaction, indicating that the accumulation of the fouling in the later stages of filtration was less than in the initial stage (0–3 min). Based on the membrane-oil droplet DLVO interaction energy in Section 3.4.1, the B20 membrane was expected to show severe fouling when filtering CTAB stabilized O/W emulsions over 20 min. However, the positive DLVO interaction energy between the CTAB-stabilized oil droplets and the deposited oil layer on the B20 membrane alleviates the membrane fouling. However, during the filtration, it was found that there was no decline in the slope of the TMP curve (Fig. 3). The possible reasons would be that the filtration time of each cycle was too short (20 min) to develop the oily cake layer, and that the drag force/crossflow could reduce the generation of the cake layer. Thus, the membrane surface was not fully covered with the cake layer and the fouling mechanism was the combination of the pore blocking (membrane-oil interaction) and the cake filtration (oil droplet-oil droplet interaction). For these two types of fouling, the oil-membrane interaction dominated over the oil-oil interactions, confirmed by the surface SEM images and Energy Dispersive X-ray (EDX) mapping images of the B0 and B20 membranes. This is particularly apparent for the B20 membrane, where the oil coverage area on the surface (35 %) was smaller than the clean membrane surface area (65 %) (Fig. 10). In contrast, the B0 membrane had a higher oil coverage of 46 %, indicating that oil-membrane interactions influenced 54 % of the surface, while oil-oil interactions accounted for the remaining 46 %. The calculation of the total DLVO interaction energies were based on the percentage of oil-oil and oil-membrane interactions [67]. For example, in SDS-stabilized emulsions at 1 mM salinity, the DLVO interaction barrier for the oil-membrane interaction for the B0 and B20 membranes were 7529 kT and 4536 kT, respectively. The DLVO interaction for the oil-oil interaction was 15,012 kT. Thus, under the combined fouling mechanism, the total DLVO interaction energy barriers for the B0 and B20 membranes were 10,135 kT and 9354 kT, respectively. Moreover, Fig. 9e indicates that the XDLVO interaction

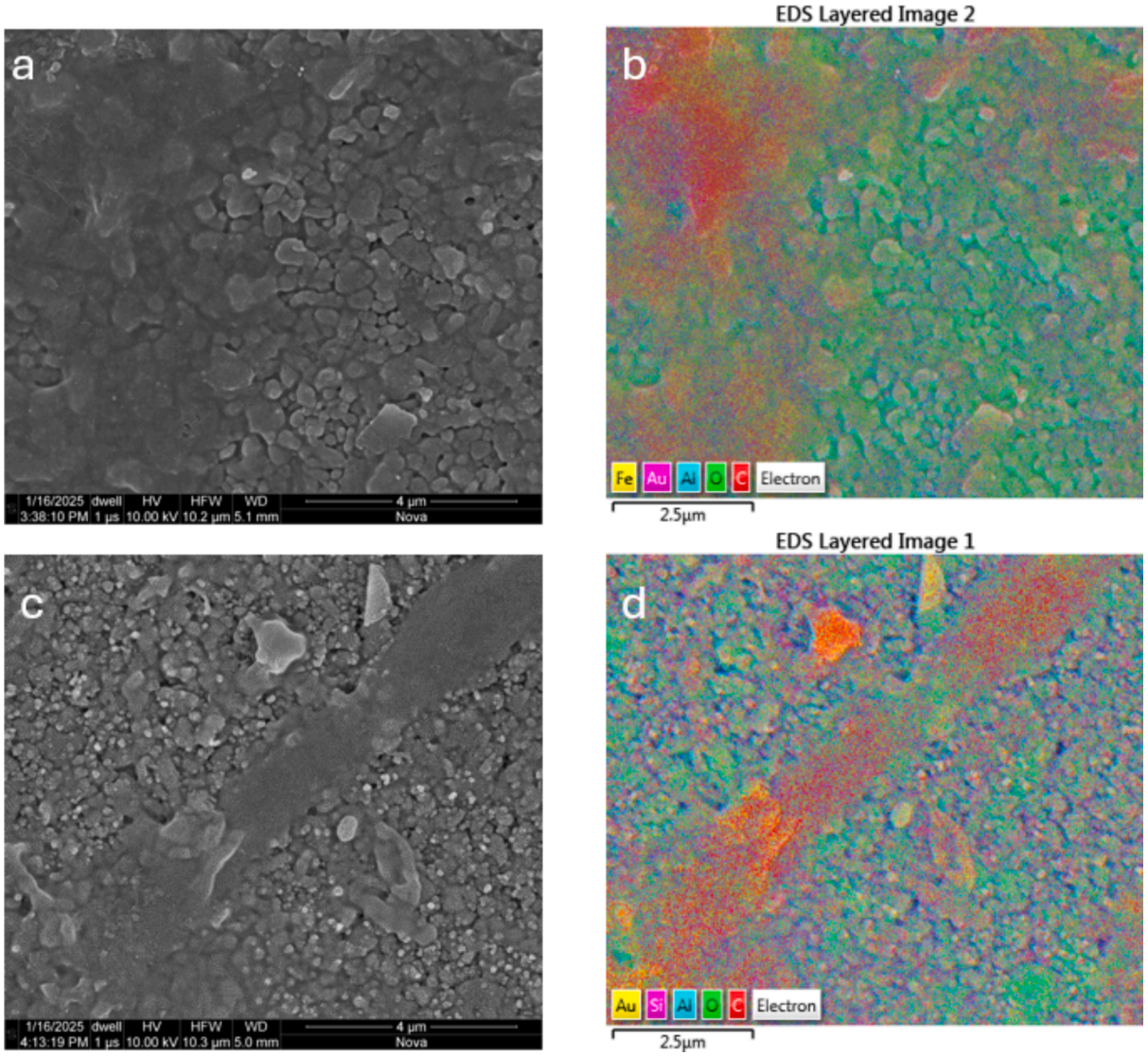

Fig. 10. (a) Surface SEM images of the fouled B0 membrane following a 20 min filtration cycle; (b) Corresponding EDX mapping images; (c) Surface SEM images of the fouled B20 membrane and (d) Corresponding EDX mapping images.

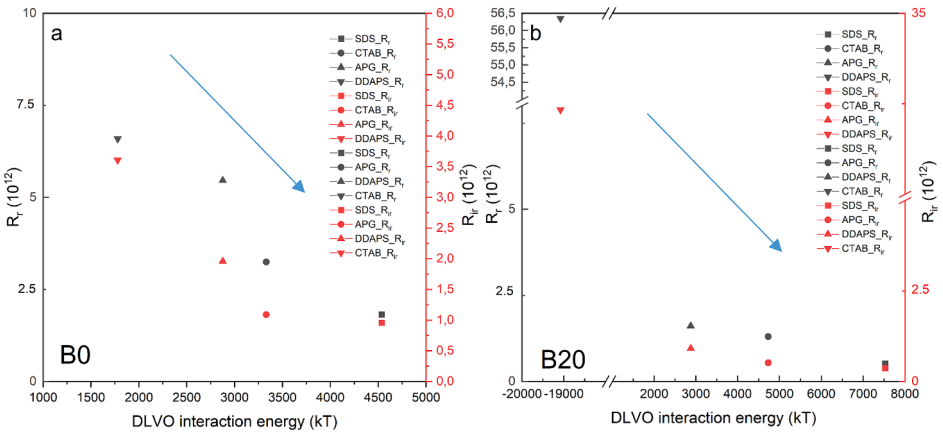

Fig. 11. The relationship between the DLVO interaction energy of the membrane-oil droplet surface interaction at the separation distance of 1 nm and the membrane fouling resistance for (a) the B0 membrane and (b) the B20 membrane filtrating 500 mg/L micron-sized O/W emulsions at 1 mM salinity. The red marks represent the irreversible fouling, and the black marks represent the reversible fouling.

energy barrier was slightly positive due to the dominance of the AB component. This XDLVO energy barrier is smaller than the oil-membrane XDLVO interaction energy barrier, indicating a higher fouling tendency. This finding is consistent with results from the fouling experiment. Thus, the XDLVO model better predicted the fouling at the later stage of the fouling experiment.

3.4.3. DLVO model and membrane fouling resistance

As shown in Fig. 11, the connection between the DLVO interaction energy of the oil droplet-membrane surface interaction and the membrane fouling resistance is illustrated, using a separation distance of 1 nm, as proposed by Lin et al. [66]. Based on the DLVO theory, a positive repulsive interaction energy between a membrane and an oil droplet indicates the alleviation of membrane fouling, while a negative value suggests an attractive effect that could increase membrane fouling. The B0 membrane exhibited a positive DLVO interaction energy for all types of the surfactants, while the B20 membrane also showed a higher positive value for the emulsions stabilized by the negatively charged SDS, APG, DDAPS. Meanwhile, as indicated by the direction of the blue arrow (from top left to the bottom right), both B0 and B20 membranes showed that reversible and irreversible fouling decreased with increased DLVO interaction energy, owing to the higher electrostatic repulsive interactions with negatively charged emulsions. The electrostatic interaction was the primary contributor to the DLVO interaction energy. A similar phenomenon can be observed at the salinity of 20 mM (Fig.S6) and 100 mM (Fig.S7). These findings offer valuable insights into reducing membrane fouling after the SiC coating at various salinities and surfactant types, attributed to the higher positive value of DLVO interaction energy.

3.5. Limitations and Recommendations

DLVO and XDLVO models cannot consider the effects of drag and shear forces. Although XDLVO is a more complex model for identifying the total interaction energy and membrane fouling, the AB compound dominates the XDLVO total energy value, ignoring the contributions of LW and EL compounds and obscuring the fouling tendencies of various O/W emulsions. Therefore, the DLVO model can better predict and compare the fouling of various O/W emulsions, particularly for the foulant-membrane interactions at higher salinity. During the filtration experiments, a single foulant-membrane interaction may not fully represent the overall interactions near the membrane surface, as multiple interactions, such as foulant-foulant interaction, also occur. Additionally, the electricity-enhanced electrified SiC membrane is recommended for future studies to mitigate fouling, given the dominance of EL interaction energy. In this study, the average surface roughness for the B0 and B20 membranes is slightly increased, with values of 55 ± 3 nm and 76 ± 3 nm, respectively (Fig. S8). Therefore, the effect of the surface roughness of the B0 and B20 membrane on the DLVO/XDLVO model was not considered in this study.

4. Conclusion

Utilizing DLVO models to quantify the interaction between the micro-sized oil droplets and the B0/B20 membrane helped predict the membrane fouling at the same hydrodynamic conditions. Variations in hydrodynamic effects were reduced by maintaining consistent crossflow velocities and permeate fluxes. In constant flux crossflow experiments, the B20 membrane had less reversible and irreversible membrane fouling than the B0 membrane when filtrating O/W emulsions stabilized with negatively charged surfactants (SDS, APG, and DDAPS). Additionally, the B20 membrane exhibited higher DLVO interaction energies than the B0 membrane. The EL components, which have the longest interaction range, mainly influence membrane fouling. In contrast, the LW and AB components, which act as the middle and short-range force, have little impact on membrane fouling. Notably, both the (X)DLVO interaction energies between the membrane and oil droplets strongly aligned with the reversible and irreversible fouling at a low salinity of 1 mM. At higher salinities (20 and 100 mM), the DLVO model also aligned well with the observed fouling trends for both B0 and B20 membranes. Additionally, the (X)DLVO model indicated that an increase in salinity from 1 mM to 100 mM resulted in a decreased (X)DLVO interaction energy barrier, aligning with increased reversible and irreversible fouling during filtration with SDS, APG, and DDAPS-stabilized O/W emulsions for the B20 membrane. Conversely, the observed increase in DLVO interaction energy for CTAB-stabilized emulsion aligned with a decreased fouling propensity and lower reversible and irreversible fouling for the B20 membrane. In summary, by coupling fouling experiments with (X)DLVO modeling, this study enhances the fundamental understanding of the impact of ionic strength and surfactant types on reversible and irreversible fouling by micro-sized oil droplets in crossflow constant flux mode.

CRediT authorship contribution statement

Guangze Qin: Conceptualization, Methodology, Formal analysis, Investigation, Data curation, Software, Writing – original draft. **Hanxiao Zhou:** Conceptualization, Methodology, Data curation. **Begüm Tanis:** Conceptualization, Methodology, Supervision, Writing – review & editing. **Luuk C. Rietveld:** Supervision, Writing – review & editing.

Sebastiaan G.J. Heijman: Conceptualization, Methodology, Formal analysis, Funding acquisition, Supervision, Writing – review & editing.

Declaration of competing interest

The authors declare that they have no known competing financial interests or personal relationships that could have appeared to influence the work reported in this paper.

Acknowledgments

The authors would like to acknowledge the PhD scholarship to Guangze Qin (No.202107720060) by the China Scholarship Council. We acknowledge the lab staff (Iske Achterhuis) from the TU Twente for her assistance in measuring the surface charge of the ceramic membranes. We also acknowledge that Qi An from the faculty of Mechanical Engineering for conducting the contact angle measurements of the ceramic membranes.

Appendix A. Supplementary data

Supplementary data to this article can be found online at https://doi.org/10.1016/j.seppur.2025.133424.

Data availability

Data will be made available on request.

References

[1] H. Chang, T. Li, B. Liu, R.D. Vidic, M. Elimelech, J.C. Crittenden, *Potential and implemented membrane-based technologies for the treatment and reuse of flowback and produced water from shale gas and oil plays: A review*, Desalination 455 (2019) 34–57, https://doi.org/10.1016/j.desal.2019.01.001.

[2] A. Fakhru'l-Razi, A. Pendashteh, L.C. Abdullah, D.R. Biak, S.S. Madaeni, Z. Z. Abidin, *Review of technologies for oil and gas produced water treatment*, J. Hazard. Mater 170 (2–3) (2009) 530–551, https://doi.org/10.1016/j.jhazmat.2009.05.044.

[3] C. He, X. Wang, W. Liu, E. Barbot, R.D. Vidic, *Microfiltration in recycling of Marcellus Shale flowback water: Solids removal and potential fouling of polymeric microfiltration membranes*, J. Membr. Sci. 462 (2014) 88–95, https://doi.org/10.1016/j.memsci.2014.03.035.

[4] A. Alborzi, I.M. Hsieh, D. Reible, M. Malmali, *Analysis of fouling mechanism in ultrafiltration of produced water*, J. Water. Process. Eng. 49 (2022) 102978, https://doi.org/10.1016/j.jwpe.2022.102978.

[5] M. Jebur, Y.-H. Chiao, K. Thomas, T. Patra, Y. Cao, K. Lee, N. Gleason, X. Qian, Y. Hu, M. Malmali, S.R. Wickramasinghe, *Combined electrocoagulation-microfiltration-membrane distillation for treatment of hydraulic fracturing produced water*, Desalination 500 (2021) 114886, https://doi.org/10.1016/j.desal.2020.114886.

[6] G. Campisi, A. Cosenza, F. Giacalone, S. Randazzo, A. Tamburini, G. Micale, *Desalination of oilfield produced waters via reverse electrodialysis: A techno-economical assessment*, Desalination 548 (2023) 116289, https://doi.org/10.1016/j.desal.2022.116289.

[7] I.M. Hsieh, A.K. Thakur, M. Malmali, *Comparative analysis of various pretreatments to mitigate fouling and scaling in membrane distillation*, Desalination 509 (2021) 115046, https://doi.org/10.1016/j.desal.2021.115046.

[8] M. Malmali, P. Fyfe, D. Lincicome, K. Sardari, S.R. Wickramasinghe, *Selecting membranes for treating hydraulic fracturing produced waters by membrane distillation*, Sep. Sci. Technol. 52 (2) (2016) 266–275, https://doi.org/10.1080/01496395.2016.1244550.

[9] A. Butkovskyi, H. Bruning, S.A.E. Kools, H.H.M. Rijnaarts, A.P. Van Wezel, *Organic Pollutants in Shale Gas Flowback and Produced Waters: Identification, Potential Ecological Impact, and Implications for Treatment Strategies*, Environ. Sci. Technol 51 (9) (2017) 4740–4754, https://doi.org/10.1021/acs.est.6b05640.

[10] A. Almojjly, D. Johnson, D.L. Oatley-Radcliffe, N. Hilal, *Removal of oil from oil-water emulsion by hybrid coagulation/sand filter as pre-treatment*, J. Water. Process. Eng. 26 (2018) 17–27, https://doi.org/10.1016/j.jwpe.2018.09.004.

[11] C. Wang, Y. Lu, C. Song, D. Zhang, F. Rong, L. He, *Separation of emulsified crude oil from produced water by gas flotation: A review*, Sci. Total. Environ 845 (2022) 157304, https://doi.org/10.1016/j.scitotenv.2022.157304.

[12] O. Samuel, M.H.D. Othman, R. Kamaludin, O. Sinsamphanh, H. Abdullah, M. H. Puteh, T.A. Kurniawan, T. Li, A.F. Ismail, M.A. Rahman, J. Jaafar, T. El-Badawy, S. Chinedu Mamah, *Oilfield-produced water treatment using conventional and membrane-based technologies for beneficial reuse: A critical review*, J. Environ. Manage 308 (2022) 114556, https://doi.org/10.1016/j.jenvman.2022.114556.

[13] S.O. Ganiyu, S. Sable, M. Gamal El-Din, *Advanced oxidation processes for the degradation of dissolved organics in produced water: A review of process performance, degradation kinetics and pathway*, Chem. Eng. J. 429 (2022) 132492, https://doi.org/10.1016/j.cej.2021.132492.

[14] G. Qin, Y. Liu, L.C. Rietveld, S.G.J. Heijman, *Oilfield-produced water treatment with SiC-coated alumina membranes*, Sep. Purif. Technol. 362 (2025) 131841, https://doi.org/10.1016/j.seppur.2025.131841.

[15] S.E. Weschenfelder, M.J.C. Fonseca, B.R.S. Costa, C.P. Borges, *Influence of the use of surfactants in the treatment of produced water by ceramic membranes*, J. Water. Process. Eng. 32 (2019) 100955, https://doi.org/10.1016/j.jwpe.2019.100955.

[16] X. Zhu, A. Dudchenko, X. Gu, D. Jassby, *Surfactant-stabilized oil separation from water using ultrafiltration and nanofiltration*, J. Membr. Sci. 529 (2017) 159–169, https://doi.org/10.1016/j.memsci.2017.02.004.

[17] T.A. Trinh, Q. Han, Y. Ma, J.W. Chew, *Microfiltration of oil emulsions stabilized by different surfactants*, J. Membr. Sci. 579 (2019) 199–209, https://doi.org/10.1016/j.memsci.2019.02.068.

[18] D. Lu, T. Zhang, J. Ma, *Ceramic membrane fouling during ultrafiltration of oil/water emulsions: roles played by stabilization surfactants of oil droplets*, Environ. Sci. Technol 49 (7) (2015) 4235–4244, https://doi.org/10.1021/es505572y.

[19] J.M. Dickhout, E. Virga, R.G.H. Lammertink, W.M. de Vos, *Surfactant specific ionic strength effects on membrane fouling during produced water treatment*, J. Colloid. Interface. Sci. 556 (2019) 12–23, https://doi.org/10.1016/j.jcis.2019.07.068.

[20] J.M. Dickhout, J. Moreno, P.M. Biesheuvel, L. Boels, R.G.H. Lammertink, W.M. de Vos, *Produced water treatment by membranes: A review from a colloidal perspective*, J. Colloid. Interface. Sci 487 (2017) 523–534, https://doi.org/10.1016/j.jcis.2016.10.013.

[21] E. Virga, R.W. Field, P.M. Biesheuvel, W.M. De Vos, *Theory of oil fouling for microfiltration and ultrafiltration membranes in produced water treatment*, J. Colloid. Interface. Sci. 621 (2022) 431–439, https://doi.org/10.1016/j.jcis.2022.04.039.

[22] B. Zhang, R. Zhang, D. Huang, Y. Shen, X. Gao, W. Shi, *Membrane fouling in microfiltration of alkali/surfactant/polymer flooding oilfield wastewater: Effect of interactions of key foulants*, J. Colloid. Interface. Sci 570 (2020) 20–30, https://doi.org/10.1016/j.jcis.2020.02.104.

[23] Z. He, S. Kasemset, A.Y. Kirschner, Y.H. Cheng, D.R. Paul, B.D. Freeman, *The effects of salt concentration and foulant surface charge on hydrocarbon fouling of a poly (vinylidene fluoride) microfiltration membrane*, Water. Res 117 (2017) 230–241, https://doi.org/10.1016/j.watres.2017.03.051.

[24] T. Zhang, Q. Wang, Y. Yang, L. Hou, W. Zheng, Z. Wu, Z. Wang, *Revealing the contradiction between DLVO/XDLVO theory and membrane fouling propensity for oil-in-water emulsion separation*, J. Hazard. Mater 466 (2024) 133594, https://doi.org/10.1016/j.jhazmat.2024.133594.

[25] M.B. Asif, Z. Zhang, *Ceramic membrane technology for water and wastewater treatment: A critical review of performance, full-scale applications, membrane fouling and prospects*, Chem. Eng. J. 418 (2021) 129481, https://doi.org/10.1016/j.cej.2021.129481.

[26] E. Eray, V. Boffa, M.K. Jørgensen, G. Magnacca, V.M. Candelario, *Enhanced fabrication of silicon carbide membranes for wastewater treatment: From laboratory to industrial scale*, J. Membr. Sci. 606 (2020) 118080, https://doi.org/10.1016/j.memsci.2020.118080.

[27] Y. Wei, Z. Xie, H. Qi, *Superhydrophobic-superoleophilic SiC membranes with micro-nano hierarchical structures for high-efficient water-in-oil emulsion separation*, J. Membr. Sci. 601 (2020) 117842, https://doi.org/10.1016/j.memsci.2020.117842.

[28] Z. Wu, Z. Ma, T. Zhu, Y. Wang, N. Ma, W. Ji, P. Nian, N. Xu, S. Zhang, Y. Wei, *Engineering of ceramic membranes with superhydrophobic pores for different size water droplets removal from water-in-oil emulsions*, Sep. Purif. Technol. 353 (2025) 128293, https://doi.org/10.1016/j.seppur.2024.128293.

[29] Q. Gu, T.C.A. Ng, Y. Bao, H.Y. Ng, S.C. Tan, J. Wang, *Developing better ceramic membranes for water and wastewater Treatment: Where microstructure integrates with chemistry and functionalities*, Chem. Eng. J. 428 (2022) 130456, https://doi.org/10.1016/j.cej.2021.130456.

[30] G. Qin, A. Jan, Q. An, H. Zhou, L.C. Rietveld, S.G.J. Heijman, *Chemical vapor deposition of silicon carbide on alumina ultrafiltration membranes for filtration of microemulsions*, Desalination 582 (2024) 117655, https://doi.org/10.1016/j.desal.2024.117655.

[31] Z. Yin, R.J.E. Yeow, Y. Ma, J.W. Chew, *Link between interfacial interaction and membrane fouling during organic solvent ultrafiltration of colloidal foulants*, J. Membr. Sci. 611 (2020) 118369, https://doi.org/10.1016/j.memsci.2020.118369.

[32] A.Y. Kirschner, Y.-H. Cheng, D.R. Paul, R.W. Field, B.D. Freeman, *Fouling mechanisms in constant flux crossflow ultrafiltration*, J. Membr. Sci. 574 (2019) 65–75, https://doi.org/10.1016/j.memsci.2018.12.001.

[33] H.J. Tanudjaja, V.V. Tarabara, A.G. Fane, J.W. Chew, *Effect of cross-flow velocity, oil concentration and salinity on the critical flux of an oil-in-water emulsion in microfiltration*, J. Membr. Sci. 530 (2017) 11–19, https://doi.org/10.1016/j.memsci.2017.02.011.

[34] H.T. Lay, C.S. Ong, R. Wang, J.W. Chew, *Choice of DLVO approximation method for quantifying the affinity between latex particles and membranes*, J. Membr. Sci. 666 (2023) 121121, https://doi.org/10.1016/j.memsci.2022.121121.

[35] M. Wang, J. Wang, J. Jiang, *Membrane Fouling: Microscopic Insights into the Effects of Surface Chemistry and Roughness*, Adv. Theor. Simul. 5 (1) (2022) 2100395, https://doi.org/10.1002/adts.202100395.

[36] X. Zhao, R. Zhang, Y. Liu, M. He, Y. Su, C. Gao, Z. Jiang, *Antifouling membrane surface construction: Chemistry plays a critical role*, J. Membr. Sci. 551 (2018) 145–171, https://doi.org/10.1016/j.memsci.2018.01.039.

[37] B.C. Huang, Y.F. Guan, W. Chen, H.Q. Yu, *Membrane fouling characteristics and mitigation in a coagulation-assisted microfiltration process for municipal wastewater*

pretreatment, Water. Res 123 (2017) 216–223, https://doi.org/10.1016/j.watres.2017.06.080.
[38] J. Xing, H. Liang, C.J. Chuah, Y. Bao, X. Luo, T. Wang, J. Wang, G. Li, S.A. Snyder, *Insight into Fe(II)/UV/chlorine pretreatment for reducing ultrafiltration (UF) membrane fouling: Effects of different natural organic fractions and comparison with coagulation*, Water. Res 167 (2019) 115112, https://doi.org/10.1016/j.watres.2019.115112.
[39] M. Ariza, J. Benavente, *Streaming potential along the surface of polysulfone membranes: a comparative study between two different experimental systems and determination of electrokinetic and adsorption parameters*, J. Membr. Sci. 190 (1) (2001) 119–132, https://doi.org/10.1016/S0376-7388(01)00430-6.
[40] X. Wang, K. Sun, G. Zhang, F. Yang, S. Lin, Y. Dong, *Robust zirconia ceramic membrane with exceptional performance for purifying nano-emulsion oily wastewater*, Water. Res. 208 (2022) 117859, https://doi.org/10.1016/j.watres.2021.117859.
[41] L. Yan, P. Li, W. Zhou, Z. Wang, X. Fan, M. Chen, Y. Fang, H. Liu, *Shrimp Shell-Inspired Antifouling Chitin Nanofibrous Membrane for Efficient Oil/Water Emulsion Separation with In Situ Removal of Heavy Metal Ions*, ACS. Sustain. Chem. Eng. 7 (2) (2019) 2064–2072, https://doi.org/10.1021/acssuschemeng.8b04511.
[42] H. Zhan, T. Zuo, R. Tao, C. Chang, *Robust tunicate cellulose nanocrystal/palygorskite nanorod membranes for multifunctional oil/water emulsion separation*, ACS Sustain. Chem. Eng. 6 (8) (2018) 10833–10840, https://doi.org/10.1021/acssuschemeng.8b02137.
[43] N.A. Ahmad, P.S. Goh, Z. Abdul Karim, A.F. Ismail, *Thin film composite membrane for oily waste water treatment: recent advances and challenges*, Membranes (Basel) 8 (2018), https://doi.org/10.3390/membranes8040086.
[44] M.W. Sulek, T. Wasilewski, *Tribological properties of aqueous solutions of alkyl polyglucosides*, Wear 260 (1–2) (2006) 193–204, https://doi.org/10.1016/j.wear.2005.02.047.
[45] P. Le Clech, B. Jefferson, I.S. Chang, S.J. Judd, *Critical flux determination by the flux-step method in a submerged membrane bioreactor*, J. Membr. Sci. 227 (1–2) (2003) 81–93, https://doi.org/10.1016/j.memsci.2003.07.021.
[46] S.P. Beier, G. Jonsson, *Critical flux determination by flux-stepping*, AIChE. J 56 (7) (2009) 1739–1747, https://doi.org/10.1002/aic.12099.
[47] J.A. Brant, A.E. Childress, *Assessing short-range membrane–colloid interactions using surface energetics*, J. Membr. Sci. 203 (1–2) (2002) 257–273, https://doi.org/10.1016/S0376-7388(02)00014-5.
[48] H. Hong, W. Peng, M. Zhang, J. Chen, Y. He, F. Wang, X. Weng, H. Yu, H. Lin, *Thermodynamic analysis of membrane fouling in a submerged membrane bioreactor and its implications*, Bioresour. Technol 146 (2013) 7–14, https://doi.org/10.1016/j.biortech.2013.07.040.
[49] C. Van Oss, *Hydrophobicity of biosurfaces—origin, quantitative determination and interaction energies*, Colloids. Surf. B. Biointerfaces 5 (3–4) (1995) 91–110, https://doi.org/10.1016/0927-7765(95)01217-7.
[50] S. Bhattacharjee, A. Sharma, P.K. Bhattacharya, *Estimation and Influence of Long Range Solute. Membrane Interactions in Ultrafiltration*, Ind. Eng. Chem. Res. 35 (9) (1996) 3108–3121, https://doi.org/10.1021/ie9507843.
[51] S.A. Onaizi, *Effect of salinity on the characteristics, pH-triggered demulsification and rheology of crude oil/water nanoemulsions*, Sep. Purif. Technol. 281 (2022) 119956, https://doi.org/10.1016/j.seppur.2021.119956.
[52] J.M. Dickhout, J.M. Kleijn, R.G. Lammertink, W.M. De Vos, *Adhesion of emulsified oil droplets to hydrophilic and hydrophobic surfaces–effect of surfactant charge, surfactant concentration and ionic strength*, Soft. Matter 14 (26) (2018) 5452–5460, https://doi.org/10.1039/C8SM00476E.
[53] G. Chen, W. Xie, C. Chen, Q. Wu, S. Qin, B. Liu, *Preparation of High Flux Chlorinated Polyvinyl Chloride Composite Ultrafiltration Membranes with Ternary Amphiphilic Copolymers as Anchor Pore-Forming Agents and Enhanced Anti-Fouling Behavior*, Ind. Eng. Chem. Res. 62 (3) (2023) 1390–1403, https://doi.org/10.1021/acs.iecr.2c03847.
[54] R. Briandet, J.-M. Herry, M.-N. Bellon-Fontaine, *Determination of the van der Waals, electron donor and electron acceptor surface tension components of static Gram-positive microbial biofilms*, Colloids. Surf. B. Biointerfaces 21 (4) (2001) 299–310, https://doi.org/10.1016/S0927-7765(00)00213-7.
[55] Y. Wang, B. Ma, M. Ulbricht, Y. Dong, X. Zhao, *Progress in alumina ceramic membranes for water purification: Status and prospects*, Water. Res 226 (2022) 119173, https://doi.org/10.1016/j.watres.2022.119173.
[56] J. Wei, P. Nian, Y. Wang, X. Wang, Y. Wang, N. Xu, Y. Wei, *Preparation of superhydrophobic-superoleophilic ZnO nanoflower@SiC composite ceramic membranes for water-in-oil emulsion separation*, Sep. Purif. Technol. 292 (2022) 121002, https://doi.org/10.1016/j.seppur.2022.121002.
[57] G. Zuo, R. Wang, *Novel membrane surface modification to enhance anti-oil fouling property for membrane distillation application*, J. Membr. Sci. 447 (2013) 26–35, https://doi.org/10.1016/j.memsci.2013.06.053.
[58] M. Chen, S.G.J. Heijman, M.W.J. Luiten-Olieman, L.C. Rietveld, *Oil-in-water emulsion separation: Fouling of alumina membranes with and without a silicon carbide deposition in constant flux filtration mode*, Water. Res 216 (2022) 118267, https://doi.org/10.1016/j.watres.2022.118267.
[59] Y. Zhao, D. Lu, Y. Cao, S. Luo, Q. Zhao, M. Yang, C. Xu, J. Ma, *Interaction Analysis between Gravity-Driven Ceramic Membrane and Smaller Organic Matter: Implications for Retention and Fouling Mechanism in Ultralow Pressure-Driven Filtration System*, Environ. Sci. Technol 52 (23) (2018) 13718–13727, https://doi.org/10.1021/acs.est.8b03618.
[60] L. Zhao, X. Qu, M. Zhang, H. Lin, X. Zhou, B.Q. Liao, R. Mei, H. Hong, *Influences of acid-base property of membrane on interfacial interactions related with membrane fouling in a membrane bioreactor based on thermodynamic assessment*, Bioresour. Technol 214 (2016) 355–362, https://doi.org/10.1016/j.biortech.2016.04.080.
[61] Z. Yang, X.-H. Ma, C.Y. Tang, *Recent development of novel membranes for desalination*, Desalination 434 (2018) 37–59, https://doi.org/10.1016/j.desal.2017.11.046.
[62] R.N. Lerner, Q. Lu, H. Zeng, Y. Liu, *The effects of biofilm on the transport of stabilized zerovalent iron nanoparticles in saturated porous media*, Water. Res 46 (4) (2012) 975–985, https://doi.org/10.1016/j.watres.2011.11.070.
[63] Q. Xie, A. Saeedi, E. Pooryousefy, Y. Liu, *Extended DLVO-based estimates of surface force in low salinity water flooding*, J. Mol. Liq. 221 (2016) 658–665, https://doi.org/10.1016/j.molliq.2016.06.004.
[64] J. Brant, *Colloidal adhesion to hydrophilic membrane surfaces*, J. Membr. Sci. 241 (2) (2004) 235–248, https://doi.org/10.1016/j.memsci.2004.04.036.
[65] S. Liang, J. Zou, L. Meng, K. Fu, X. Li, Z. Wang, *Impacts of high salinity on antifouling performance of hydrophilic polymer-modified reverse osmosis (RO) membrane*, J. Membr. Sci. 708 (2024) 123042, https://doi.org/10.1016/j.memsci.2024.123042.
[66] T. Lin, J. Zhang, W. Chen, *Recycling of activated carbon filter backwash water using ultrafiltration: Membrane fouling caused by different dominant interfacial forces*, J. Membr. Sci. 544 (2017) 174–185, https://doi.org/10.1016/j.memsci.2017.09.028.
[67] J. Liu, T. Huang, R. Ji, Z. Wang, C.Y. Tang, J.O. Leckie, *Stochastic collision-attachment-based monte carlo simulation of colloidal fouling: transition from foulant-clean-membrane interaction to foulant-fouled-membrane interaction*, Environ. Sci. Technol 54 (19) (2020) 12703–12712, https://doi.org/10.1021/acs.est.0c04165.